A re-appraisal of the proposed rapid Matuyama-Brunhes geomagnetic reversal in the Sulmona Basin, Italy

M. E. Evans[1] and A. R. Muxworthy[2]

[1] Department of Physics, University of Alberta, Edmonton, Alberta, T6G 2G7, Canada. E-mail: tedevans.evans403@gmail.com

[2] Department of Earth Science and Engineering, Imperial College London, London, SW7 2AZ, UK

SUMMARY

An extremely sharp magnetic reversal observed in lacustrine sediments in central Italy has been interpreted as a record of the Matuyama-Brunhes geomagnetic polarity reversal that may represent less than a decade (Sagnotti et al., 2014. 2016). Here, we report new results from the same Sulmona Basin outcrop that question this interpretation. In particular, we find evidence of reversed (Matuyama) directions well above the proposed Matuyama-Brunhes Boundary (MBB). Coercivity spectra of anhysteretic remanent magnetization (ARM) imply a 3-component magnetic mineralogy: low-, intermediate-, and high-coercivity. The low-coercivity component is found in all but one of the samples and carries a strong modern overprint seen throughout the section. The high-coercivity component is dominated by volcanic material which is prone to remagnetization. Since it is much more magnetic than the surrounding lacustrine sediments, it may influence the remanence signal even when present at very low concentrations. The intermediate-coercivity component is the main carrier of any true primary remanence, but whether or not this can be isolated depends on the blocking-temperature and coercivity spectra of individual samples, and on the demagnetization method used. The complexity of the magnetization, the reversed zones above the proposed MBB, and the normal zones that Sagnotti and

colleagues found below it, lead to the conclusion that this section does not carry a reliable high-resolution record of the geomagnetic field. Thus, we feel that inferences about the stratigraphic position and duration of the MBB are premature.

Introduction

It is firmly established that the geomagnetic field stochastically reverses its polarity over geological time, which offers an important window on the dynamics of the Earth's interior. But it also provides an extremely useful geological chronometer–the geomagnetic polarity timescale (GPTS), based on the established age of each reversal. An excellent summary is given by Gee & Kent (2007). Despite these advances, many questions remain. One of the most persistent difficulties has been the determination of the time needed for a polarity reversal to take place. From a global summary of sedimentary records of the four most recent reversals, Clement (2004) concludes that the average time required for the polarity switch is close to 7000 years, with individual sites yielding estimates ranging from ~2000 to ~10000 years. In stark contrast, Sagnotti et al. (2016) describe a remanence polarity inversion—interpreted as a record of the Matuyama-Brunhes Boundary (MBB)—that may have lasted less than a decade. Brown et al. (2007) explore a geomagnetic model based on a global summary of archaeomagnetic and palaeomagnetic data covering the last 7000 years (CALS7K2, Korte & Constable, 2005), and find that "rapid reversals on subdecadal timescales are seen for a small number of locations". This surprising result could have important ramifications for the behaviour of the earth's core,

and it is therefore imperative to scrutinize any relevant observations to ensure that whatever inferences are made rest on secure empirical evidence. The observations reported by Sagnotti et al. (2016) are such a case. The data in question were obtained from a continuous sequence of lacustrine sediments outcropping in the Sulmona Basin in central Italy. Samples kindly provided by Sagnotti and colleagues have enabled us to take a closer look. The new data reveals a more complex directional pattern that we do not regard as a true record of geomagnetic field behaviour. Instead, we argue that it is corrupted by pervasive normal overprints.

Samples and Methods

Two sets of samples were available for the experiments described in this paper. The first consists of pristine samples from the original collection made by Sagnotti et al. (2016). They correspond to Figure 12 of that paper. The second set comprises samples cut in Edmonton from blocks collected in May 2016 by Leonardo Sagnotti, Biagio Giaccio, and one of us (MEE). A total of 53 samples were investigated, spanning an interval of 51 cm bracketing the proposed MBB. Stratigraphic heights are measured from the base of tephra layer SUL2-19, as was done by Sagnotti et al. (2016). Sample volumes range from 4 to 8 cc. Natural remanent magnetization (NRM) and anhysteretic remanent magnetization (ARM) were measured at the University of Alberta on a 2G cryogenic magnetometer equipped with an alternating-field (AF) demagnetizer. ARM's were acquired in a 100 mT peak AF with a steady bias field of 100 μT. Thermal demagnetization experiments were carried out in an ASC Model TD48-SC oven also at the University of Alberta. High-temperature susceptibility measurements

were made at Imperial College London using an Agico KLY-2 Kappabridge fitted with a CS2 furnace. Heating was conducted in air and in Ar to help assess chemical alteration. First-order reversal curve (FORC) measurements were made using a Princeton Measurement Vibrating Sample Magnetometer at Imperial College London.

To establish a basis for comparison with the earlier results of Sagnotti et al. (2014, 2016), we subjected 26 samples to AF demagnetization and 7 to thermal demagnetization. As a further test, we subjected 20 samples to a combination of thermal demagnetization up to 300°C, followed by alternating-field demagnetization up to 100 mT. The maximum temperature of 300 °C was chosen to be high enough to remove most (if not all) of the modern overprint, and low enough to avoid chemical alteration. All demagnetization results were assessed by PuffinPlot freeware (Lurcock & Wilson, 2012), and by the PMGSC software kindly provided by R.J. Enkin of the Geological Survey of Canada.

Results

Natural remanent magnetization

Representative results obtained from the three demagnetization techniques used (AF, TH, and TH+AF) are illustrated in Figure 1. In all cases, a recent overprint is removed in the first few steps. The sample at 51 cm (Fig. 1a) is an example of AF demagnetization revealing underlying normal polarity. The sample at 20 cm (Fig. 1b) starts out at an intermediate direction (suggesting that the recent overprint is not strong enough to pull the NRM completely into the modern field), but subsequently reveals a clear reversed-polarity magnetization. Figure 1c shows

that the sample at 25 cm has a strong recent overprint, and thermal demagnetization shows normal polarity throughout. But an embedded reversed component is clearly revealed between 290 and 399°C (vector difference direction: D=176°, I=-56°), followed by a return to normal polarity at higher temperatures. Thermal results for the sample at 19 cm (Fig. 1d) show an intermediate initial direction (like the adjacent sample at 20 cm), but further demagnetization again reveals an underlying reversed component between 290 and 399°C. For the TH+AF method, the sample at 3 cm (Fig. 1e) has normal polarity throughout, whereas the sample at 18 cm (Fig. 1f) starts from an intermediate direction and then moves to reversed polarity.

Overall, the demagnetization results for the entire collection are ~~very good~~ straightforward. After removal of the modern overprint, coherent underlying magnetic components are revealed on vector end-point plots. ~~The~~ For these, the ~~mean~~ median value for MAD (maximum angular deviation) ~~value~~ is 4°, but eight MAD values range between 11° and 19°. The 'cleaned' inclination values ~~results~~ are shown as a stratigraphic profile in Figure 2, which also includes the corresponding data of Sagnotti et al. (2016). The two datasets will be discussed in more detail below, after the rock magnetic experiments have been described.

Anhysteretic remanence

Natural sediments almost always contain mixed assemblages of several distinct mineral components. To probe the magnetic composition of the Sulmona samples we carried out AF demagnetization experiments on ARMs given to 17 representative samples (Fig. 3). One of these (T19) is a small chip of tephra SUL2-19 that was too small and irregular to be used in NRM experiments. The others were selected from samples that had not been heated. As a whole, AF

demagnetization of ARM illustrates a smooth gradation from magnetically soft material to magnetically hard material, with intermediate curves probably representing mixtures. We pursue this possibility by analysing the AF demagnetization curves using the method of Heslop & Dillon (2007). This approach unmixes the curves into end-members determined from the data–not input by the user. For our samples, their procedure indicates that three end-members suffice: magnetically soft (EM1), intermediate (EM2), and hard (EM3) (Fig. 4a). The relative proportions of these components present in each sample are presented stratigraphically in Figure 4b. As expected from visual inspection of the AF curves, EM3 is prevalent (87%) in the tephra sample T19. But it is also present in significant amounts up to 10 cm, and near the tephra SUL2-18 (~28 cm). Minor amounts of EM3 are observed at other elevations. The low-coercivity component EM1 is present throughout the section, although sample T19 has very little (4%), and it is not detectable at all at a height of 3 cm. Elsewhere it comprises about 25-50% in most samples. The intermediate component (EM2) is present in all samples, falling mostly between ~45% and ~65%, except for the tephra horizons (SUL2-18, 28%; SUL2-19, 9%).

High-temperature susceptibility

High-temperature susceptibility curves were determined for eight samples spread throughout the section, chosen to represent a wide range of end-member compositions. Two examples are shown in Figure 5. Generally, the data were noisy due to the low magnetic signals, but the trends are still clear. Both samples indicate that magnetite is the dominant magnetic mineral present, which is also true for the other six samples. But heating to 700°C causes variable amounts of

chemical alteration. The change is modest for the sample at 3 cm (Fig. 5a), but more marked for the sample at 12 cm (Fig. 5b). Heating in an argon atmosphere suppresses the alteration in some, but not all, cases. This being so, we ran an additional experiment to determine the temperature at which alteration begins (Fig. 5c). First, the sample was heated to 250°C and then cooled down to room temperature, then to 450°C, and finally to 550°C. The curves obtained are reversible (Fig. 5c) indicating that alteration does not occur until temperatures above 550 °C.

FORC measurements

FORC measurements were carried out for eight samples, two of which are illustrated in Figure 6. The SUL2-19 tephra sample (T19, Fig. 6a) is an excellent example of single-domain (SD) behaviour with a peak at ~30 mT and an extended distribution stretching beyond 60 mT. But there is also a minor peak at the lowest fields, indicating the presence of multidomain (MD) grains. The sample at 12 cm yields a similar SD-like diagram (Fig. 6b), but with a more restricted distribution peaking at ~15 mT and an MD peak near the origin. The small (MD) peaks near the origin presumably reflect EM1 contributions, whereas the main (SD) peaks correspond to mixtures of EM2 and EM3. As would be expected, the volcanic content endmember (EM3) is greater in the tephra.

Discussion

All samples carry a modern overprint with coercivities up to ~20 mT, but in some cases a divergent direction is initially observed because the overprint is relatively weak (e.g. Fig. 1d). However, the majority of samples yield NRM

directions loosely grouped around the geocentric axial dipole direction expected at the site. This modern overprint can be attributed to EM1, which we interpret as consisting predominantly of MD magnetite.

The directions revealed after removal of the modern overprint show significant differences between the Rome and Edmonton results (Fig. 2). Above 26 cm, the Rome AF data are exclusively of normal polarity, whereas the TH+AF Edmonton data indicate several reversely-magnetized horizons. Four of these between 28 cm and 36.5 cm are shown in Figure 7. Three other horizons above tephra SUL2-18 (at 30, 42, and 44 cm) have normal-polarity remanence, but show systematic movement towards shallow directions as demagnetization proceeds (Fig. 8). We take this as evidence for an underlying reversed-polarity component that cannot be fully resolved. This suggestion is supported by data from lower in the section, near tephra layer SUL2-19. Sagnotti et al. (2014) regard the normal polarities they observed near this tephra (and the one below it, SUL2-20) as Brunhes-age overprints. We concur, but argue that the systematic movement we see at 4.5 cm (Fig. 8) provides evidence for the Matuyama reversed-polarity signal expected at this stratigraphic height. Given the evidence for reversed polarity above SUL2-18, we carefully reviewed our AF data and found a hint of reversed polarity at 49 cm. Between 10 and 25 mT, the sample in question has normal polarity (D=11.0°, I=56.0°, MAD=6.4°, n=4), but a poorly constrained component with negative inclination is revealed between 25 and 40 mT (D=197.2°, I=-72.2°, MAD=9.0°, n=4), beyond which the remanence becomes unstable.

Turning now to the crucial stratigraphic interval where Sagnotti et al. (2014, 2016) find the polarity flip they interpret as the MBB. We find that the two

polarity states overlap so that no single polarity boundary can be established. For example, of the three samples centred on 26 cm, one has normal polarity and two have reversed. The normal polarity result (D=14.4°, I=52.2°, MAD=2.9°, 20-35 mT, n=4) was obtained by AF demagnetization, and agrees with the polarity found by Sagnotti et al. (2016). One of the reversed polarities was obtained by thermal demagnetization (D=187.7°, I=-50.4°, MAD=8.3°, 290-399°C, n=4), the other by the TH+AF method (D=178.1°, I=-51.3°, MAD=7.9°, 30-80 mT, n=5). However, both samples at 28 cm were subjected to the TH+AF method and yet they yield opposite polarities. It seems that once the modern overprint is removed, there may still be a delicate balance between two opposed magnetic components that are very difficult to separate. The results obtained will depend on the relative amounts of the three end-members present and their coercivity and blocking-temperature spectra. Consequently, different demagnetization schemes may yield different outcomes. The two samples at 28 cm illustrate this. The normal-polarity sample has higher blocking temperatures, whereas the remanence of the other sample decreases more rapidly (Fig. 9). In the former, decay is monotonic and directions are normal throughout (100°C-30 mT, D=26.0°, I=63.0°, MAD=4.0°, n=10). In the latter, the remanence vector moves smoothly from the normal overprint direction to an underlying reversed component (see Fig. 7), passing through a broad intensity minimum as the overprint is removed and the reversed component begins to dominate the net remanence remaining.

As pointed out above, the modern overprint is predominantly carried by EM1, with coercivities mostly below 20 mT. At the other end of the spectrum, Figure 3 indicates that the high-coercivity component (EM3) can be firmly

associated with volcanic input. Sagnotti et al. (2014) point out that the volcanic input is associated with Brunhes-age normal-polarity overprints near SUL2-19 and SUL2-20, and Sagnotti et al. (2016) regard this as one of two explanations for the normal-polarity horizons near SUL2-18, the other being that they are a genuine Brunhes record. The identification of underlying reversed components (Fig. 7) favours the overprint option, so that all three tephra (and the sediments near them) carry what we interpret as a Brunhes overprint. But the exact mechanism responsible for such a high-coercivity overprint remains unknown. We consider three possiblities, but acknowledge that there may be others. (1) A recently acquired viscous magnetization like the modern overprint residing in EM1. (2) The growth of new magnetic minerals linked in some way to the volcanic input. (3) Delayed lock-in. Mechanism (1) can be ruled out on the grounds that EM3 is dominated by high-coercivity SD magnetite that is unlikely to be prone to viscous remagnetization. The currently available information cannot distinguish between (2) and (3), but for the present purposes this poses no great problem. Both mechanisms involve SD magnetite grains, either created at some post-depositional time (2), or present in the original volcanic fallout (3). Either way, if the delay is long enough, it is possible to generate Brunhes-age overprints. For mechanism (3), we suggest that many of the the tiny (sub-micron) SD particles of EM3 are free to rotate in interstitial water for a significant time after deposition (i.e. they have high magnetic stability, but low mechanical stability). This could also happen in mechanism (2), but it is much less likely because the particles involved will be locked to the parent tephra grains – either as surface growth rims or as internal inclusions. Peaks in NRM and ARM associated with tephra layers and the sediments near them indicate that EM3 is

strongly magnetic. Indeed, at 3 cm elevation (immediately above tephra SUL2-19) we obtain an NRM value of 179 mA/m, compared to a median value below 1 mA/m for samples more than a few centimetres away from tephra layers. This indicates that a small fraction of EM3 could significantly affect the remanence of a sample, and raises the presence of volcanic EM3 remanence – acquired long after deposition – as a potentially widespread feature in the Sulmona Basin. The situation has some similarity to that seen in the Chinese loess, where differential lock-in introduces considerable complexity into magnetostratigraphic profiles. For example, Spassov et al. (2003) identify seven full polarity changes at the MBB, spanning a stratigraphic thickness of ~40 cm. They also conclude that the observed downward displacement of the MBB implies a time delay in excess of 20,000 years. For the Sulmona basin, Sagnotti et al. (2014) report $^{40}Ar/^{39}Ar$ ages for several tephra layers. Linear interpolation between two of these (SUL2-22: 791.9±1.9 ka and SUL2-16: 781.3±2.3 ka) implies an age of 786.1 ka for the proposed MBB. This is about 13,000 years older than the 773 ka obtained from a comprehensive global analysis (Singer, 2014). This conflict could be reconciled if significant (>10 kyr) lock-in delay occurred. This is not unreasonable, given that the ~30 cm between the normal-polarity overprint near SUL2-20 and the suggested lowest Brunhes horizon implies a delay of at least 1500 years.

Given that the remanences carried by EM1 and EM3 are both thought to be later remagnetizations, we are left with the intermediate component EM2 as the possible recorder of any primary geomagnetic signal. Fortunately, it occurs in all but one of the samples and accounts for ~45% to ~65% of the ARMs (Fig. 4b). But whether or not the true signal can be isolated depends on the coercivity and blocking-temperature spectra of individual samples.

Conclusions

We find evidence of reversed polarity above the MBB proposed by Sagnotti et al. (2014, 2016), whereas they find evidence of normal polarity below it (as do we). Taken together, these observations suggest that this stratigraphic section carries a complex magnetic signal. We conclude that the observed magnetic pattern, as a whole, is not an accurate record of geomagnetic field behaviour. Thus, the claim that the Matuyama-Brunhes transition lasted no more than about a decade cannot be regarded as firmly established.

Acknowledgements

We are enormously indebted to Leonardo Sagnotti and Biagio Giaccio for their help and guidance at all stages of this study. This work was funded by a Royal Society International Exchanges grant to ARM and MEE.

References

Brown, M.C., Holme, R. & Bargery, A. (2007) Exploring the influence of the non-dipole field on magnetic records for field reversals and excursions. Geophys., J. Int. 168, 541-550. doi: 10.1111/j.1365-246X.2006.03234.x

Clement, B. M. (2004) Dependence of the duration of geomagnetic polarity reversals on site latitude. Nature, 428, 637-640. doi:10.1038/nature02459.

Gee, G.S. & Kent, D.V. (2007) Source of Oceanic Magnetic Anomalies and the Geomagnetic Polarity Timescale: In: Kono, M., (Ed.) Geomagnetism, Treatise on Geophysics, vol. 5, pp. 455–507.

Heslop, D. & Dillon, M. (2007) Unmixing magnetic remanence curves without a priori knowledge. Geophysical Journal International 170, 556-566. doi:10.1111/j.1365-246X.2007.03432.x

Korte, M. & Constable, C.G. (2005) Continuous geomagnetic field models for the past 7 millennia: 2. CALS7K. Geochemistry, Geophysics, Geosystems 6, Q02H16. doi: 10.1029/2004GC000801.

Lurcock P. C. & Wilson, G. S. (2012) PuffinPlot: A versatile, user-friendly program for paleomagnetic analysis. Geochemistry, Geophysics, Geosystems 13. doi: 10.1029/2012GC004098.

Sagnotti L., Scardia G., Giaccio B., Liddicoat J. C., Nomade S., Renne P. R. & Sprain, C. J. (2014) Extremely rapid directional change during Matuyama-Brunhes geomagnetic polarity reversal. Geophysical Journal International 199(2), 1110-1124. doi: 10.1093/gji/ggu287

Sagnotti L., Giaccio B., Liddicoat J. C., Nomade S., Renne P. R., Scardia G. & Sprain, C. J. (2016) How fast was the Matuyama-Brunhes geomagnetic reversal? A new subcentennial record from the Sulmona Basin, central Italy. Geophysical Journal International 204(2), 798-812. doi: 10.1093/gji/ggv486

Singer, B.S., A Quaternary geomagnetic instability time scale. Quaternary Geochronology 21, 29-52. http://dx.doi.org/10.1016/j.quageo.2013.10.003

Spassov, S., Heller, F., Evans, M.E., Yue, L.P. & von Dobeneck, T. (2003) A lock-in model for the complex Mauyama-Brunhes boundary record of the loess/palaeosol sequence at Lingtai (Central Chinese Loess Plateau). Geophysical Journal International, 155, 350-366.

Zhao X., Heslop D. & Roberts, A. P. (2015) A protocol for variable- resolution first-order reversal curve measurements. Geochemistry, Geophysics,

Geosystems 16(5), 1364-1377. doi:10.1002/2014GC005680.

Figure captions

Fig. 1: Examples of the three demagnetization methods used. (a,b) AF; (c, d) TH; (e, f) TH+AF. The numerical part of the name refers to the sample's stratigraphic height (in cm). Larger symbols indicate the NRM. Red points indicate the magnetic components revealed by PuffinPlot. The local geocentric axial dipole directions are plotted on each of the stereonets as a blue square.

Fig. 2: Inclination profiles for AF (light blue), TH (orange), and TH+AF (green) results. The dark blue curve shows the results obtained by Sagnotti et al. (2016), obtained by digitizing their Figure 5. Stratigraphic heights are measured from the base of tephra layer SUL2-19.

Fig. 3: AF demagnetization curves for ARM given to representative samples.

Fig. 4: End-member analysis using the procedure of Heslop & Dillon (2007). (a) Coercivity gradient curves for the three end-members. (b) End-member abundances for each sample.

Fig. 5: High-temperature susceptibility results for samples at heights of (a) 3 cm, (b) 12 cm. (c) Multi-cycle heating of the sample at 12 cm. In (c) the data for the 450 ˚C curve has been shifted up by 0.01 m^3kg^{-1} in the vertical axis, and the 550 ˚C dataset by 0.02 m^3kg^{-1}. The experiments were conducted in air. The samples were prepared by grinding into a powder. Sister samples were treated to the same heating in an Ar environment, which was found to suppress – but not eliminate – high-temperature alteration.

Fig. 6: FORC diagrams for (a) tephra SUL2-19 (sample T19), and (b) a sample at 12 cm. The irregular grid protocol of Zhao et al. (2015) was used, as the samples

were too weak to be measured using the routine regular grid. Averaging time and smoothing factor were 200 ms and 4, respectively.

Fig. 7: Behaviour of four samples at, and above, tephra layer SUL2-18 during TH+AF demagnetization. The stratigraphic height (cm) of each sample is indicated in italics. Closed (open) symbols are on the lower (upper) hemisphere. The square indicates the direction of the local geocentric axial dipole field.

Fig. 8: TH+AF behaviour of four samples that exhibit directional trajectories to shallow inclinations indicative of an unresolved reversed magnetization. The stratigraphic height of each sample is indicated in italics. Closed (open) symbols are on the lower (upper) hemisphere.

Fig. 9: Decay of NRM (normalized) during thermal demagnetization followed by alternating-field demagnetization (TH+AF) for the two samples at 28 cm. Closed symbols represent the sample that retained normal polarity throughout (NRM=3.45 mA/m). Open symbols represent the sample that ultimately revealed reversed magnetization (see Fig.7) (NRM=1.53 mA/m).

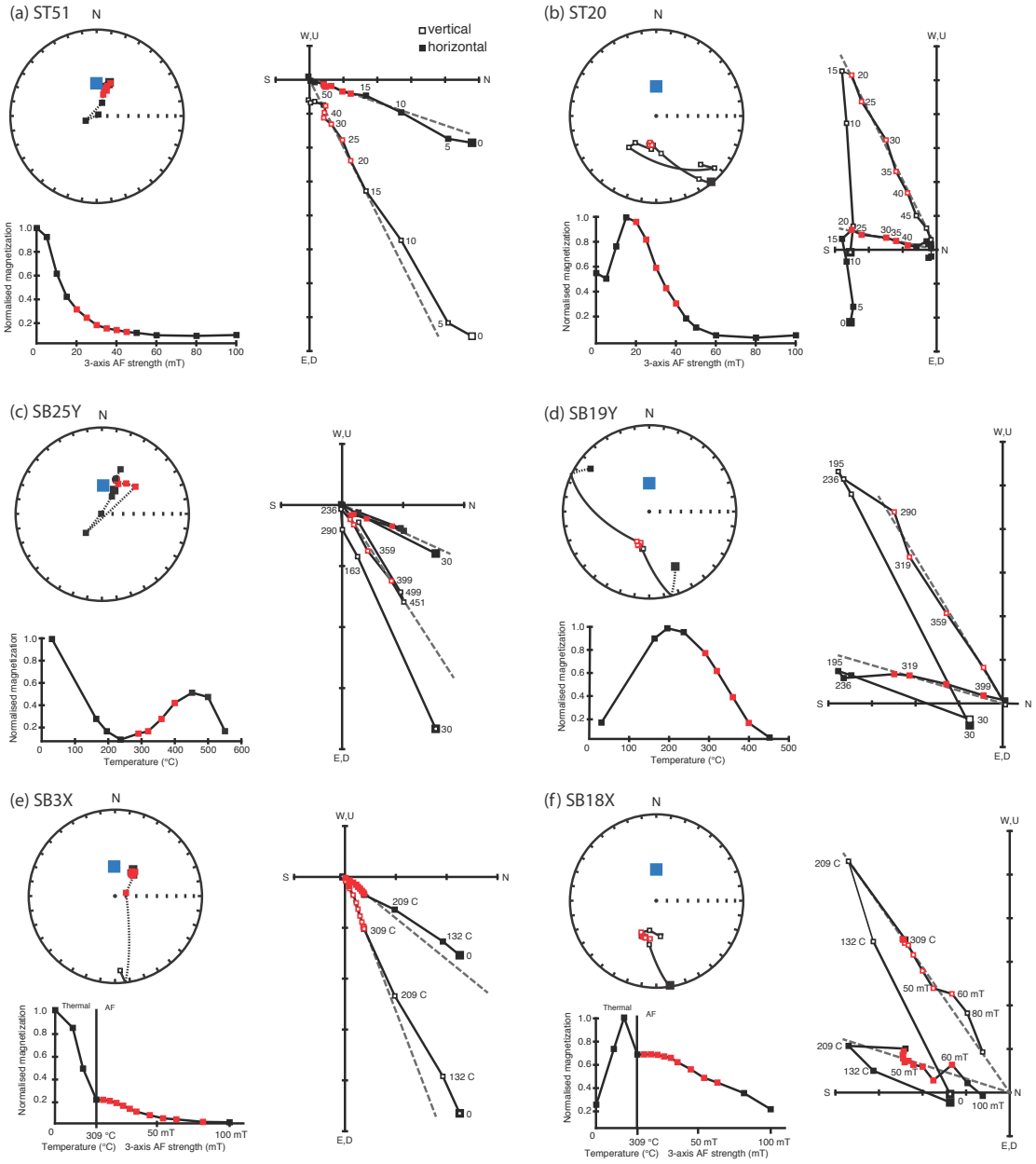

(a) ST51
N
W,U
vertical
horizontal
S
N
E,D
Normalised magnetization
3-axis AF strength (mT)
(b) ST20
(c) SB25Y
Temperature (°C)
(d) SB19Y
(e) SB3X
Thermal
AF
309 °C
50 mT
100 mT
(f) SB18X
209 C
132 C
309 C
60 mT
80 mT

Figure 1

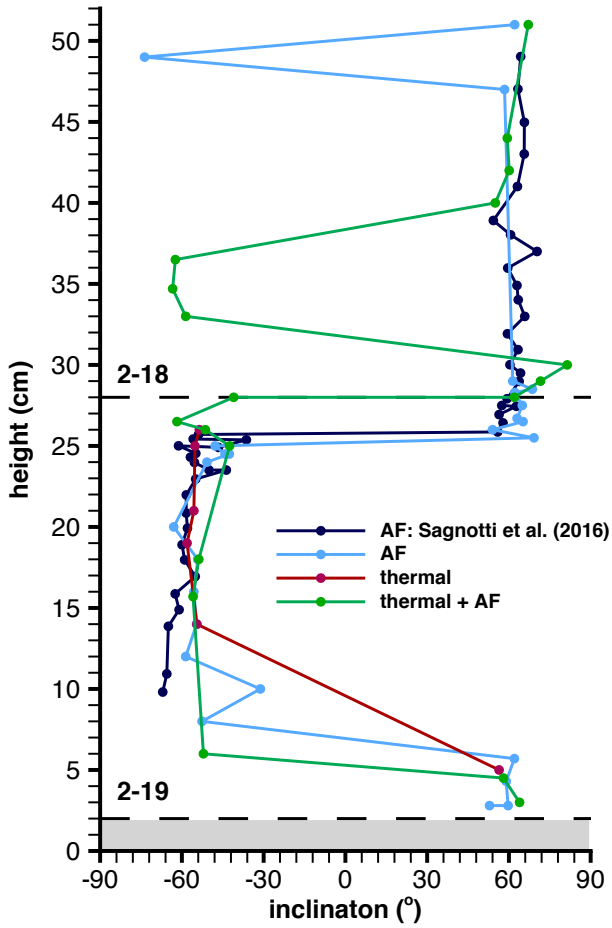


Figure 2

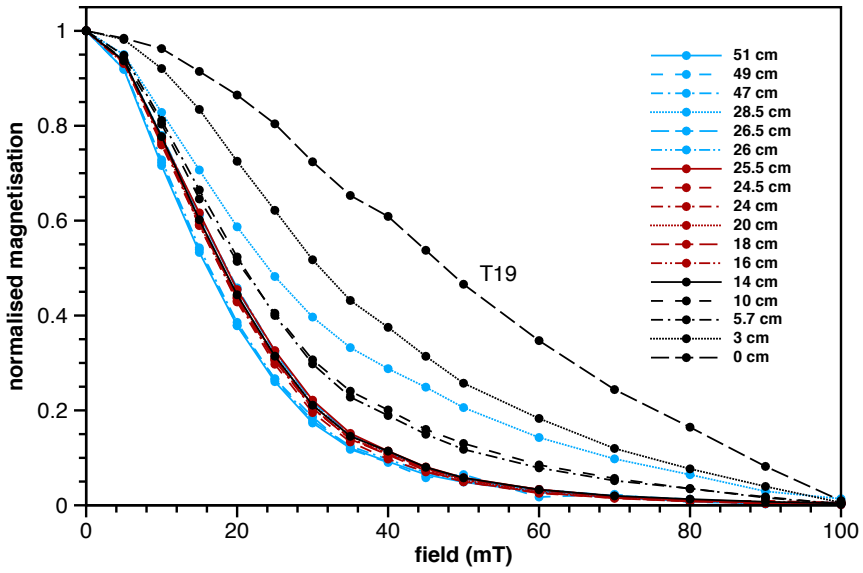


Figure 3

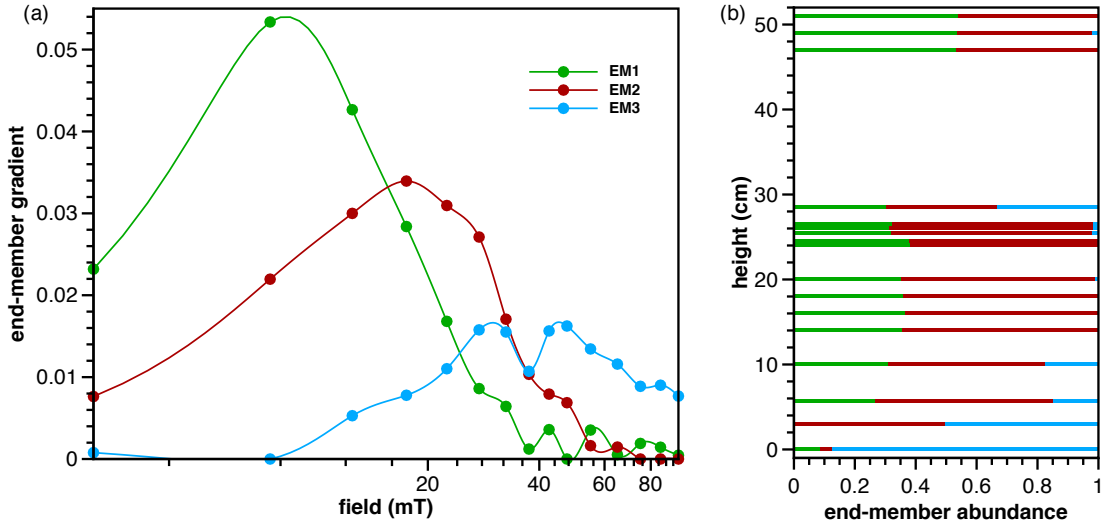


Figure 4

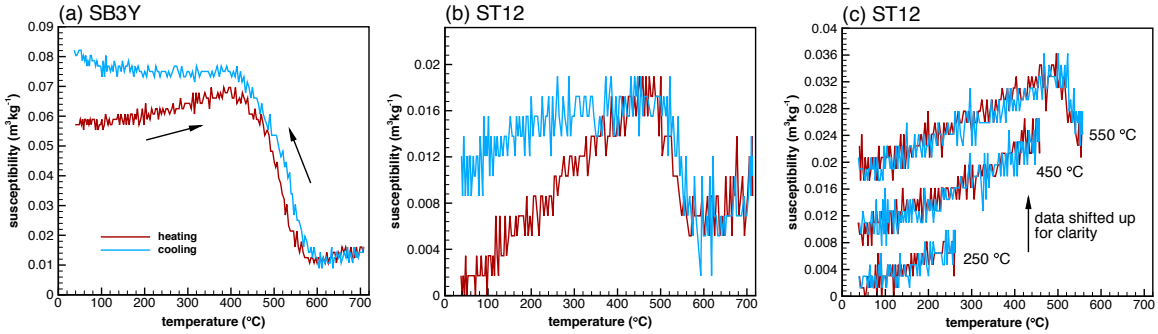


Figure 5

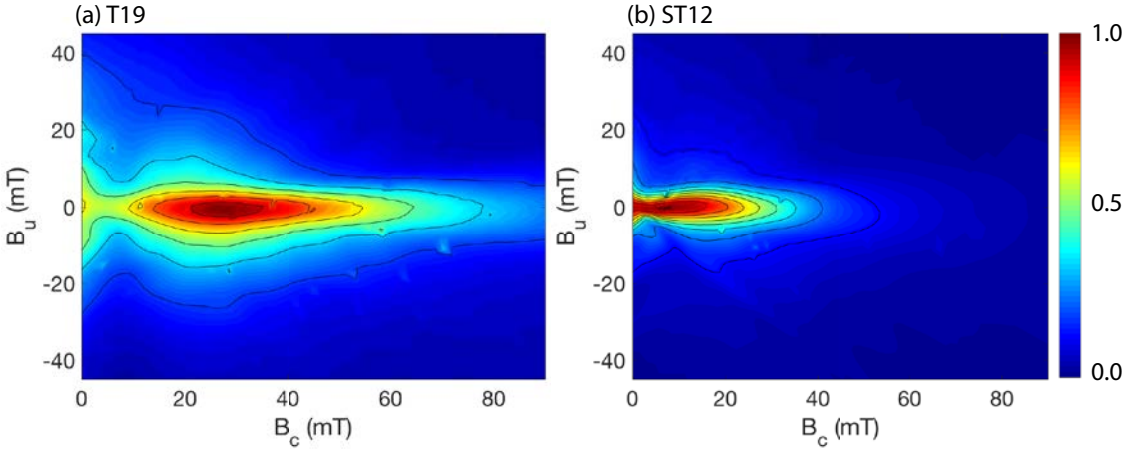


Figure 6

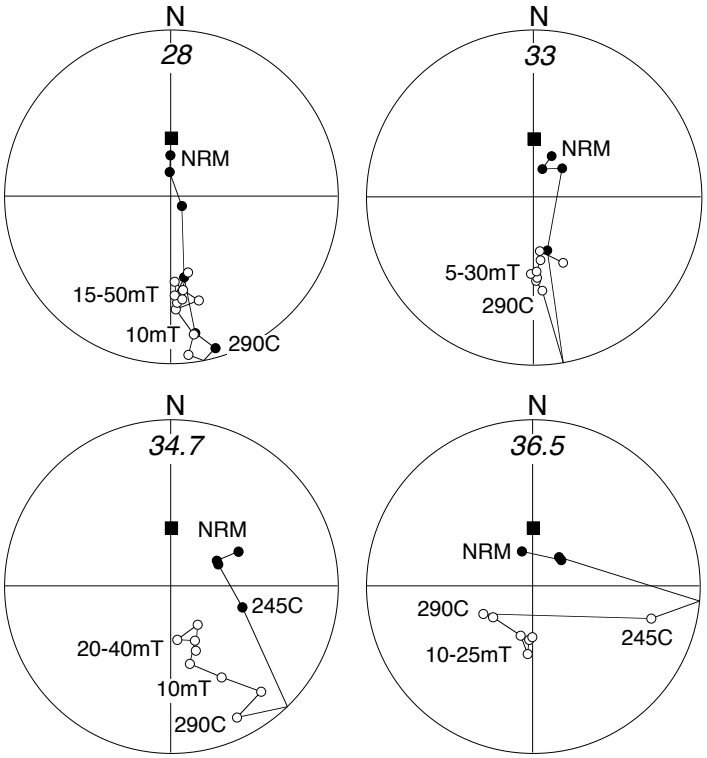

N
28
NRM
15-50mT
10mT
290C
N
33
NRM
5-30mT
290C
N
34.7
NRM
245C
20-40mT
10mT
290C
N
36.5
NRM
290C
245C
10-25mT

Figure 7

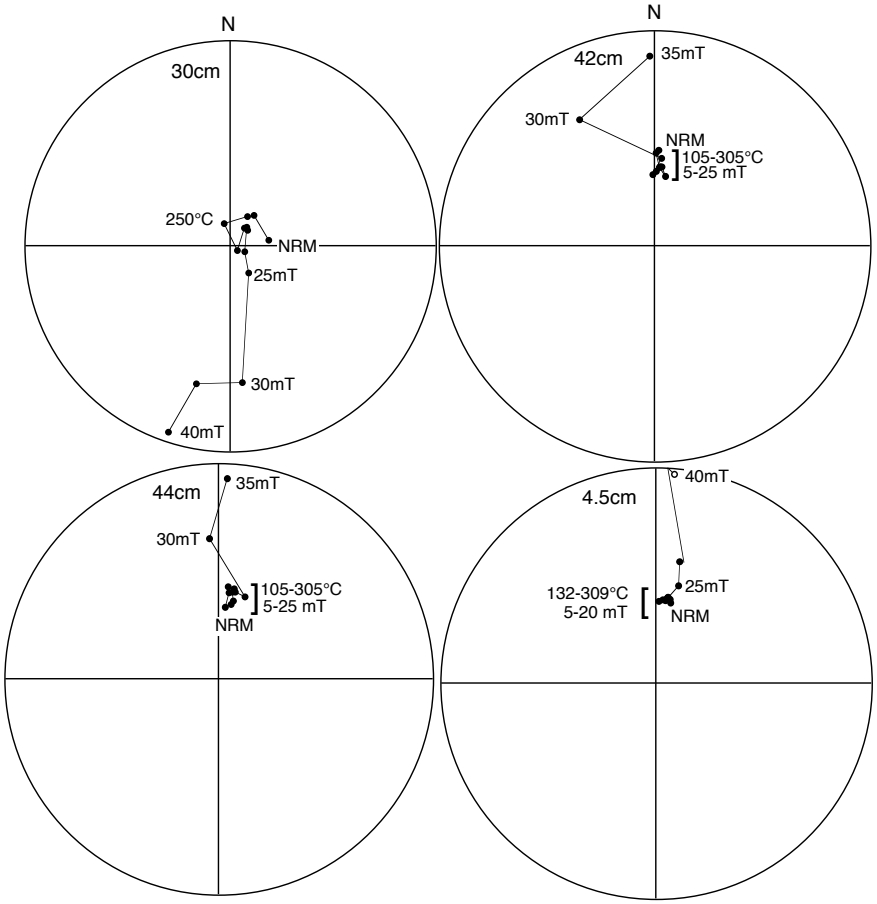

N
30cm
250°C
NRM
25mT
30mT
40mT
N
42cm
35mT
30mT
NRM
105-305°C
5-25 mT
44cm
35mT
30mT
105-305°C
5-25 mT
NRM
40mT
4.5cm
132-309°C
5-20 mT
25mT
NRM

Figure 8

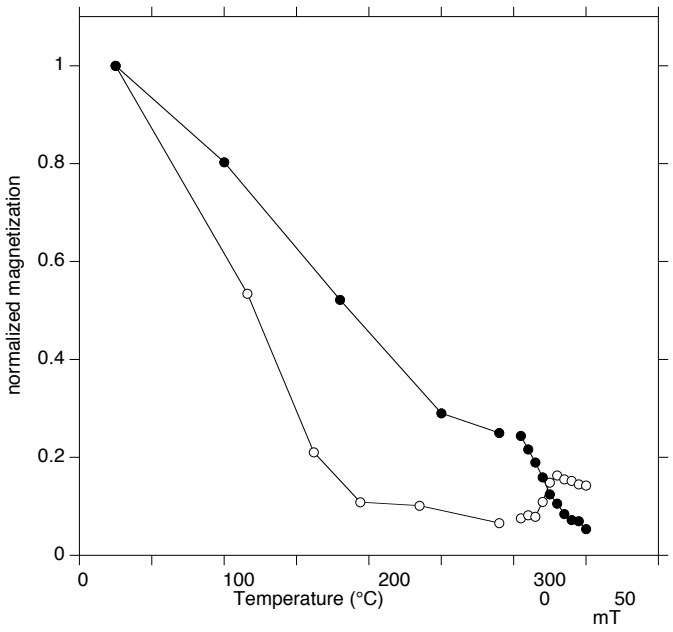

normalized magnetization
1
0.8
0.6
0.4
0.2
0
0
100
200
300
Temperature (°C)
0
50
mT

Figure 9